Structure and Nonrigid Motion Analysis of Satellite Cloud Images

Lin Zhou and Chandra Kambhamettu
Dept. of Computer and Info. Sci.
University of Delaware
Newark, Delaware, US, 19716
lzhou/chandra@cis.udel.edu

Dmitry B. Goldgof
Dept. of Computer Sci. and Eng.
University of South Florida
Tampa, Florida, US, 33620
goldgof@csee.usf.edu

Abstract

This paper proposes a new method for recovering nonrigid motion and structure of clouds under affine constraints using time-varying cloud images obtained from meteorological satellites. This problem is challenging not only due to the correspondence problem but also due to the lack of depth cues in the 2D cloud images (scaled orthographic projection). In this paper, affine motion is chosen as a suitable model for small local cloud motion. However, the cloud motion model can also be extended and not necessarily be affine. Analysis of intensity images is first used to find the candidates of correspondence for each point. Then affine motion model is utilized to find the structure (cloud-top height), motion parameters, and point correspondences. Extensive analysis has been done on defining appropriate constraints on depth that are necessary for achieving converge. Finally, experimental results on time-varying images of hurricane Luis, captured by GOES-9 satellite in geosynchronous orbit are presented. We believe that this is the first reported work on estimating structure and motion under scaled orthographic views, when the object of interest is undergoing a nonrigid motion. Our results are very encouraging, and have many potential applications especially in earth and space sciences.

1 Introduction

Developing automatic computational motion analysis algorithms capable of handling both rigid and nonrigid motion has been a difficult task. Most of the work in motion analysis [5] [14] [13] has been done based on the rigidity assumption where the shape of objects do not change over time. However, the rigidity assumption fails in numerous real-world examples, such as the dynamics of cloud, human movement, motion of biological organs and so on. A lot of potential applications make nonrigid motion analysis very desirable. However, nonrigid motion is especially hard because of its varying nature [7]. So far, most of the work in nonrigid motion analysis aims at using complete structure of the scene (stereo or range) [6] [16] [17], or optic flow estimation of 2D images [3]. Very limited studies have been conducted to recover structure and nonrigid motion at the same time from time-varying images. Balasubramanian et al. recovered 3D structure and nonrigid motion from 2D image sequences under perspective projection [1]. In this paper, we develop novel techniques for recovering structure and nonrigid motion from a sequence of 2D cloud images which are undergoing scaled orthographic projection. The motion model used in this paper is affine but it can also be extended to quadric, fluid or other general motion models.

The estimation of cloud-top structure and motion using multiple satellite views of clouds is an important application area in nonrigid motion analysis. Accurate cloud heights and motion are significant for a number of meteorological and climate applications [4] [11] such as cloud model verification, physically-based numerical weather prediction and data assimilation, and radiation balance estimation for Mission to Planet Earth type climate baseline studies. It is an extremely challenging problem due to the complex dynamics of imaging instruments and the underlying non-linear phenomena of cloud formation and weather. Also, the scaled orthographic projection in cloud images makes the structure problem more difficult. Earlier work on cloud tracking is based on 3D analysis. Authors in [15] use 3D data obtained from stereo analysis, and/or approximate 2D intensity images for depth information in order to perform cloud tracking. In this paper, however, we use 2D images to estimate not only motion but also structure. Intensity analysis is first used to find the candidates for correspondence, then affine motion model is used to find the cloud motion and also the structure.

The rest of the paper is organized as follows: In Section 2.1, nonrigid motion model is defined. In Section 2.2, we describe the error function for least-square

minimization. Issues dealing with a good initial guess are described in Section 2.3, and the correspondence problem is discussed in Section 3. Constraints on depth that ensure proper convergence are discussed in Section 4. In Section 5, we present the experimental results on cloud images obtained from GOES9 satellite in geosynchronous orbit. Finally, conclusions and future work are presented in Section 6.

2 Motion and Structure from 2D Cloud Images

Our aim is to estimate depth, nonrigid motion, and 3D point correspondence from a sequence of 2D cloud images. We will first assume that correspondences are known. The method for obtaining the correspondences will be discussed in section 3. The algebraic relations that can be used to derive structure and nonrigid motion from cloud images are explained below.

Consider a point $P^1({x_l}^1, {y_l}^1, {z_l}^1)$ in frame 1 moving to a point $P^2({x_l}^2, {y_l}^2, {z_l}^2)$ in frame 2 after a nonrigid motion and to point $P^3({x_l}^3, {y_l}^3, {z_l}^3)$ in frame 3, and so on. Let M^i, a displacement function, describes the motion between frame i and $i+1$. For cloud images, we consider them as scaled orthographic projections, since the distance between the satellite and clouds is very high (approximately 30,000 Kilometers). Thus, the structure constraints for points on cloud images are almost nothing. For point (x_l, y_l, z_l), we have the form:

$$ {X_l}^i = {x_l}^i, \quad {Y_l}^i = {y_l}^i, \tag{1} $$

where $({x_l}^i, {y_l}^i)$ is in the 3D space, $({X_l}^i, {Y_l}^i)$ is the coordinate of the point projected on the cloud image. Here we assume that the scaling for $({X_l}^i, {Y_l}^i)$ and $({x_l}^i, {y_l}^i)$ is the same. From the nature of the motion, the following equations can be derived:

$$ \begin{aligned} {x_l}^{i+1} &= M^i({x_l}^i, {y_l}^i, {z_l}^i), \\ {y_l}^{i+1} &= M^i({x_l}^i, {y_l}^i, {z_l}^i), \\ {z_l}^{i+1} &= M^i({x_l}^i, {y_l}^i, {z_l}^i) \end{aligned} \tag{2} $$

where M^i is the displacement function defining the nonrigid motion over a certain surface patch. Similar equations for every pair of successive frames can also be derived.

2.1 Nonrigid Motion Model

Cloud motion is a special case of nonrigid motion. It can be described as semi-fluid motion in which there are both partial fluid and partial solid motion. Any restricted classes of nonrigid motion, such as articulated motion, quasirigid motion, isometric motion, homothetic motion and conformal motion, will not be suitable for the cloud motion. Affine motion model is a general non-rigid motion model and has more power in describing nonrigid motion. Also, affine motion model has been experimentally proven to be a suitable model for small local cloud motion [15]. A lot of work has been done on affine motion [10] [12] [9] [8]. However, most of the work assumed correspondence [8] or did not recover structure at the same time. In this paper, we choose affine motion as the model for small local cloud motion to recover structure, nonrigid motion, and 3D point correspondence at the same time. However, the cloud motion model can also be extended and it does not necessarily have to be affine. Affine motion has 12 parameters and governed by the following relations:

$$ \begin{aligned} {x_l}^{i+1} &= a_1{x_l}^i + b_1{y_l}^i + c_1{z_l}^i + d_1, \\ {y_l}^{i+1} &= a_2{x_l}^i + b_2{y_l}^i + c_2{z_l}^i + d_2, \\ {z_l}^{i+1} &= a_3{x_l}^i + b_3{y_l}^i + c_3{z_l}^i + d_3. \end{aligned} \tag{3} $$

Then following equations can be obtained by Eq. 1 and Eq. 3:

$$ \begin{aligned} {x_l}^{i+1} &= a_1{X_l}^i + b_1{Y_l}^i + c_1{z_l}^i + d_1, \\ {y_l}^{i+1} &= a_2{X_l}^i + b_2{Y_l}^i + c_2{z_l}^i + d_2, \\ {z_l}^{i+1} &= a_3{X_l}^i + b_3{Y_l}^i + c_3{z_l}^i + d_3. \end{aligned} \tag{4} $$

According to Eq. 4, the motion between successive frames is assumed to be the same. However, it is almost impossible to guarantee above assumption to be true in cloud images. This assumption can be relaxed by a scaling factor using an additional unknown δ_i to Eq. 4 as following:

$$ \begin{aligned} {x_l}^{i+1} &= \delta_i(a_1{X_l}^i + b_1{Y_l}^i + c_1{z_l}^i + d_1), \\ {y_l}^{i+1} &= \delta_i(a_2{X_l}^i + b_2{Y_l}^i + c_2{z_l}^i + d_2), \\ {z_l}^{i+1} &= \delta_i(a_3{X_l}^i + b_3{Y_l}^i + c_3{z_l}^i + d_3). \end{aligned} \tag{5} $$

Eq. 5 is the constraint equations for tracking a point across a sequence of images using affine motion model.

2.2 Error-of-Fit Function and Minimization Method

Levenberg-Marquardt non-linear optimization method [2] is then introduced to recover structure and motion from cloud images based on above affine motion model. To make this algorithm robust and to be able to find a good solution, a good error function that measures the difference between a guessed model and given data set is very important. We first define the error function by using the distance between the

given point correspondence and the one obtained by Eq. 5:

$$EOF = \sum_{j=1}^{Mframe} \sum_{i=1}^{Ndata} ((X'_{ij} - x_{ij})^2 + (Y'_{ij} - y_{ij})^2) \quad (6)$$

where (X'_{ij}, X'_{ij}) is the given correspondence for point (X_i, Y_i) in the first frame, (x_{ij}, y_{ij}) is the correspondence obtained by Eq. 5.

One problem in Eq. 5 is how to get (X'_{ij}, Y'_{ij}), the given correspondence for point (x_i, y_i). In the following sections, we will discuss the correspondence problem in detail and give some enhanced versions of EOF function.

2.3 Initial Guess

The initial guesses for all the unknowns in Eq. 5 are required, i.e. 12 motion parameters, the depth for every point in the first frame, and δ_i for each pair of successive images. It is known that almost all non-linear system solvers are highly sensitive to initial guesses. For numerical simplicity and ensuring convergence, two eliminations of unknowns have been done in our method. For the first cloud frame in our experiments, we have a stereo occurrence. Stereo analysis of this pair of images has been done to obtain the disparities in [15]. Then, the depth unknowns in the first frame can be eliminated by fixing them with these disparities. This is very important for our algorithm. Due to the poor constraints on depth in cloud images, much more constraints on depth are necessary. Stronger constraints will be discussed in section 4. In addition, we eliminate the translational unknowns and set the translate components, i.e. d_1, d_2, d_3, to constants. These constants can be obtained by averaging the translations of the correspondence candidates and are experimentally found to yield good results. For the other nine motion parameters and δ_i, initial values are chosen assuming that cloud motion is very small between two successive frames.

parameter	*initial guess*	*parameter*	*initial guess*
a_1	1	b_3	0
a_2	0	c_1	0
a_3	0	c_2	0
b_1	0	c_3	1
b_2	1	δ_i	1

3 Correspondence Problem

In section 2, an assumption is made that the correspondence for each point is known ahead of time. However, this is a difficult problem for cloud images due to the complex dynamics of imaging instruments and the underlying non-linear phenomena of cloud formation and weather. In this paper, intensity analysis is first used to find the candidates of correspondence, then motion analysis is performed to find the best one.

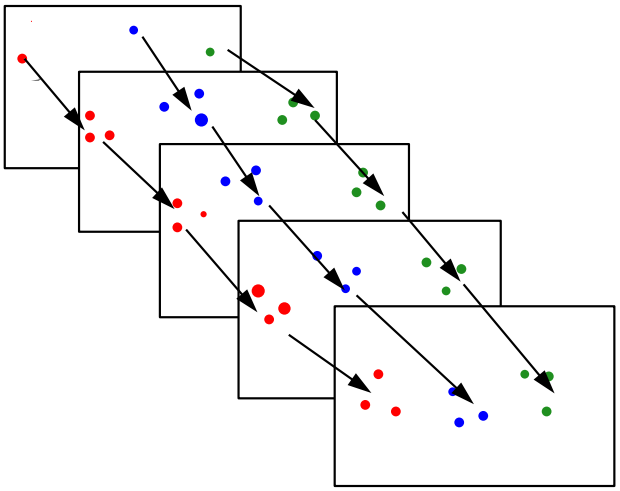

Figure 1: correspondence candidates by intensity analysis.

3.1 Correlation matching

For intensity analysis, correlation-based method is used. For each image pixel, a match score is computed between a template centered at the pixel and neighborhoods within a search area in the test image. The match score is given by,

$$\frac{\sum_{i,j}(X_{i,j} - \overline{X})(Y_{i-m,j-n} - \overline{Y_{m,n}})}{\left[\sum_{i,j}(X_{i,j} - \overline{X})\right]^{\frac{1}{2}} \left[\sum_{i,j}(Y_{i-m,j-n} - \overline{Y_{m,n}})\right]^{\frac{1}{2}}} \quad (7)$$

where $X_{i,j}$ and $Y_{i,j}$ correspond to template pixels within the reference and test images respectively. $X_{i,j}$ is the grey level of the the (i,j)th pixel within the template neighborhood of the reference image and the $Y_{i-m,j-n}$ is the grey level of (i,j)th pixel in (m,n)th search area of the test image. The value $\overline{X}$ and $\overline{Y_{m,n}}$ are the corresponding mean values. For each pixel in the reference image, the match scores for all neighborhoods within the search area are computed. Then, all the pixels within the search area of the test image are sorted by correlation match scores from high to low. The first three are chosen as the correspondence candidates in our algorithm. Fig. 1 shows this strategy.

3.2 Template and Search Windows

It is very important to make sure that correspondence candidates found are reliable. The search window size and the template window size can be controlled. In our algorithm, we specify these two window sizes as following:

Time Interval	*Template size*	*Search Area*
1	11×11	9×9
2	15×15	15×15
3	17×17	19×19
4	19×19	21×21
5	21×21	23×23
6	23×23	25×25

3.3 Find the best correspondence

With correspondence candidates, we can modify the error function as follows:

$$EOF_1 = \sum_{j=1}^{Mframe} \sum_{i=1}^{Ndata} min((X_{ij}^1 - x_{ij})^2 + (Y_{ij}^1 - y_{ij})^2, (X_{ij}^2 - x_{ij})^2 + (Y_{ij}^2 - y_{ij})^2, (X_{ij}^3 - x_{ij})^2 + (Y_{ij}^3 - y_{ij})^2)) \quad (8)$$

where (X_{ij}^1, Y_{ij}^1), (X_{ij}^2, Y_{ij}^2), (X_{ij}^3, Y_{ij}^3) are the first, second and third correspondence candidates for point (X_i, Y_i) in the first frame respectively, (x_{ij}, y_{ij}) is the correspondence estimate obtained by Eq. 5.

Brute-force method (i.e. exhaustive searching) is used by minimizing the distance between all the correspondence candidates and the one obtained by Eq. 5. By this way, motion constraints are added to the correlation-based analysis to find the best correspondence for each point.

4 Constraints

Although the depth unknowns in the first frame are eliminated by fixing them to disparities, the error function Eq. 8 will still have infinite global minima because there is no information about the change of the cloud-top height for the following frames in Eq. 8. Clearly, we need some restrictions on the the range of values the depth can take. For cloud images, intensity is a good proportional guess for depth [15]. Based on this observation, we can specify a small range for the depth of each point. This range is obtained using a proportional factor between intensity and depth. And the proportional factor can be calculated by dividing the intensity by disparity of the first frame (Note: Both the intensity and disparity are known for the first frame). Thus we have

$$z'_{ij} - a \leq z_{ij} \leq z'_{ij} + a \quad (9)$$

where z_{ij} is the depth of the ith data in the jth frame, z'_{ij} is the corresponding depth obtained from the intensity of the ith frame. $2a$ is the range for the depth. In our experiments, a is set to 2 in disparity units and was found to yield good results. Thus, we incorporate this inequality constraint into the minimization process using a penalty method.

Consider the minimization problem

$$minimize \;\; f(\vec{x}) \quad subject\ to\ \vec{x} \in S \quad (10)$$

where f is a continuous function on E^n and S is a constraint region. The penalty method replaces the above problem by an unconstrained problem of the form

$$minimize \;\; f(\vec{x}) + cP(\vec{x}) \quad (11)$$

where c is a positive constant and P is penalty function on E^n such that

1. P is continuous.
2. $P(\vec{x}) \geq 0 \;\; \forall \; \vec{x} \in E^n$ and
3. $P(\vec{x}) = 0$ if and only if $\vec{x} \in S$.

Clearly, for large values of c, the minimum of the above problem will lie in a region where P is small. We expect that as c increases, the corresponding solution will approach the feasible region S and will minimize f. In other words, we expect the solution point of Eq. 11 converges to the solution of Eq. 10 as $c \to \infty$. The penalty method asks us to solve Eq. 11 with increasing values of c. Let $[\vec{x_k}]$ denote the sequence of solutions obtained. Then any limit point of the sequence is a solution to the original Eq. 10.

With the cloud application, we found experimentally that it is sufficient to solve Eq. 11 for a single large value of c. We set c to 1000 and solve Eq. 11. It's solution satisfies Eq. 10. The value of c is defined to be 1000; this selection is arbitrary and was experimentally found to yield good results.

Given a single inequality constraint $g(\vec{x}) \leq 0$, a penalty function that satisfies the stated conditions is $P(\vec{x}) = (max\,[0, g_i(\vec{x})])^2$. We can thus rewrite our original constrained minimization problem as an unconstrained minimization problem as follows.

$$P_{ij} = \left(max\left[0, z_{ij} - (z'_{ij} + a)\right]\right)^2 + \left(max\left[0, (z'_{ij} - a) - z_{ij}\right]\right)^2. \quad (12)$$

And the problem becomes

$$minimize \sum_{j=1}^{Mframe} \sum_{i=1}^{Ndata} min((X_{ij}^1 - x_{ij})^2 + (Y_{ij}^1 - y_{ij})^2, (X_{ij}^2 - x_{ij})^2 + (Y_{ij}^2 - y_{ij})^2, (X_{ij}^3 - x_{ij})^2 + (Y_{ij}^3 - y_{ij})^2)) + cP_{ij}. \quad (13)$$

Fig. 2 illustrates the need for constraints. (a), (b) are two results of depth for five cloud images without constraints. (c) is a result with constraints. Although

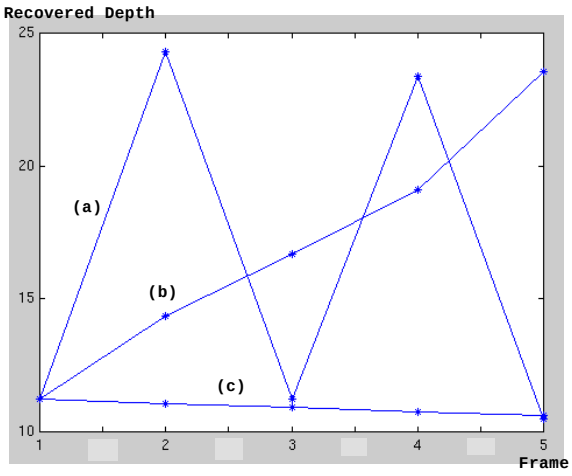

Figure 2: (a),(b): results of structure without constrains for five cloud images, (c): result of structure with constraints.

the depth is fixed in the first frame, the values for the following frames can change dramatically without constraints. The result with constraints looks smooth and all the recovered values satisfy the constraint conditions.

Due to the use of constraints, the algorithm is somewhat insensitive to initialization. However, this does not mean that we can use any arbitrary initialization. A bad initialization may lead to the plateaux problem and make the process of convergence very slow.

5 Experimental Results

In this section, we present our experimental results. Before working on the real cloud images, experiments on simulation data are performed. For the simulation data, several epllisoidal patches are generated. Nine feature points in a small patch are selected randomly on the surface, and their scaled orthographic projections are used as the input data. Without loss of generality, all motion parameters are assigned 0.1 for the initial guess. The algorithm seems very robust and yields very good results. The following tables show the recovered motion parameters and also the depths of the last frame for one set of data.

parameter	*initial guess*	*fit result*	*true value*
a_1	0.1	0.9000	0.9
a_2	0.1	0.1000	0.1
a_3	0.1	0.1000	0.1
b_1	0.1	0.2000	0.2
b_2	0.1	0.8000	0.8
b_3	0.1	0.1000	0.1
c_1	0.1	0.1000	0.1
c_2	0.1	0.1000	0.1
c_3	0.1	0.7000	0.7
average error	NA	0.0000	NA

point	*recovered depth*	*ground truth*
z_1	69.9690	69.9690
z_2	69.9694	69.9694
z_3	69.9696	69.9696
z_4	78.3721	78.3721
z_5	78.3726	78.3726
z_6	78.3729	78.3729
z_7	88.6230	88.6230
z_8	88.6230	88.6230
z_9	88.6237	88.6237

We have then performed experiments on the Geostationary satellite image sequences of clouds. We have used the image sequences acquired by the GOES-9 satellite in a super-rapid scan mode. The data includes 490 frames of a remarkable 1-minute image time series of hurricane Luis from NASA-Goddard. All the images are mostly taken every minute starting from 09-06-95 at 1023 UTC to 09-06-95 at 2226 UTC. Though five spectral bands are available for each frame, only visible channel having 10-bits per pixel are being used for our experiments. We will be using the other spectra to see for their use in determining the structure and motion in our future experiments. In this paper, we just give the results for a sequence of 11 cloud images (from 1621 UTC to 1634 UTC). We have a stereo occurrence with Goes-8 images for 1621 UTC and 1634 UTC. Stereo analysis of these pairs have been done on a Maspar parallel machine, using a coarse-to-fine, hierarchical algorithm which was previously developed at NASA-Goddard [15]. As we mentioned before, we use the disparities of 1621 UTC to eliminate the depth unknowns in the first image (1621 UTC). Fig. 3 shows the intensity image of 1621 UTC. In order to make our algorithm clear, here we just concentrate on the small region within the red circle in Fig. 3. For this small region, nonrigid motion and structure within the following 11 frames (from 1621 UTC to 1634 UTC) are recovered. The results for nine points are given here. Fig. 4(a) shows the original positions of the nine points in the first frame, and

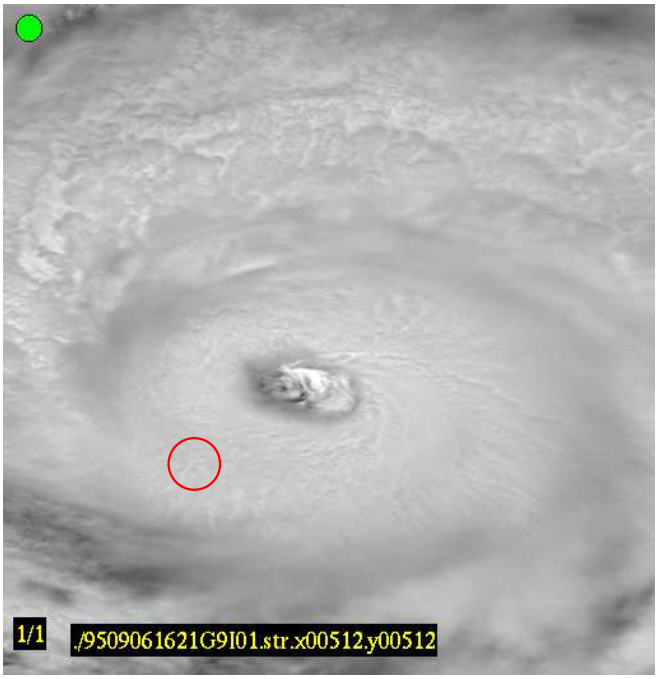

Figure 3: The intensity image for 1621 UTC (Note: experiments are performs on the small region within the circle).

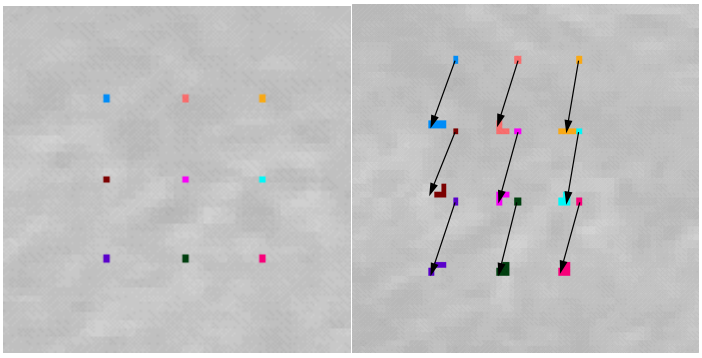

Figure 4: (a): Nine points are selected within a small region in 1621 UTC image. (b): Three candidates for each points in 1634 UTC, then motion analysis is added to find a best one (Note: The arrows point to the best correspondence after motion analysis).

Fig. 4(b) shows the correspondence candidates and the recovered correspondence in the last frame, i.e. 1634 UTC. According to the results, It is clear that the best correspondence is obtained by combining the intensity and motion analysis.

The results for the depth in 1634 UTC and motion parameters are given in following tables. We can see the recovered depths for 1634 UTC are very close to the disparities obtained by stereo analysis.

parameter	*recovered value*	*parameter*	*recovered value*
a_1	1.0046	δ_2	1.0029
a_2	-0.0014	δ_3	1.0052
a_3	-0.0047	δ_4	1.0041
b_1	-0.0018	δ_5	1.0034
b_2	0.9997	δ_6	1.0014
b_3	0.0015	δ_7	1.0091
c_1	-0.0004	δ_8	0.9939
c_2	-0.0008	δ_9	1.0034
c_3	1.0080	δ_{10}	1.0029
δ_1	1.0028	*average error*	0.3763

point	*disparity*	*recovered depth*
z_1	10.0119	9.5113
z_2	9.97037	9.0003
z_3	9.98052	9.0271
z_4	9.53351	9.5690
z_5	9.95377	10.0582
z_6	9.65637	8.9710
z_7	9.99402	9.4993
z_8	10.4667	9.9135
z_9	9.70109	10.2246

6 Conclusion and Future Work

This paper presents the recovery of structure and nonrigid motion from a sequence of 2D cloud images. The main contribution of this research is that it not only deals with the problem of recovering structure from the scaled orthographic projection views but also performs nonrigid motion estimation to get correspondences by combining intensity and motion analysis. The results are very encouraging and has tremendous applications in space science, especially in cloud models for weather prediction. This work can also be easily applied for data under perspective projections such as lip motion, human facial expression, hand motion, tongue motion and so on. Our future work involves using this algorithm in cloud models developed at NASA-Goddard and analyzing its feasibility. Much more experiments on the cloud images will be performed. Every grid point for each image can be tested to get the whole cloud structure. Also instead of dis-

parity, IR is used to eliminate the depth unknowns for improving cloud analysis performance. Our final goal is to have a set of techniques that can perform cloud tracking, nonrigid motion and structure analysis for climate studies efficiently.

Acknowledgments

Research funding was provided by the National Science Foundation Grant NSF IRI-9619240. The authors are thankful to Dr. Fritz Hasler of NASA Goddard and Dr. K. Palaniappan of University of Missouri-Columbia for providing the data.

References

[1] Ramprasad Balasubramanian, Dmitry B. Goldgof, and Chandra Kambhamettu. Tracking of nonrigid motion and 3d structure from 2d image sequences without correspondences. *ICIP'98*, Octobor, 1998.

[2] A. Bjorck. Least squares methods. 2:465–647, 1990.

[3] A. Giachetti and V. Torre. Optical flow and deformable objects. *Proceeding of 5th ICCV*, pages 706–711, 1995.

[4] A. F. Hasler. Stereoscopic measurements. In P. K. Rao, S. J. Holms, R. K. Anderson, J. Winston, and P. Lehr, editors, *Weather Satellites: Systems, Data and Environmental Applications, Section VII-3*, pages 231–239. Amer. Meteor. Soc., Boston, MA, 1990.

[5] T. S. Huang. Motion analysis. In *Encyclopedia of Artificial Intelligence*, volume 1, pages 620–632. John Wiley and Sons, New York, 1986.

[6] Chandra Kambhamettu, Dmitry B. Goldgof, and Matthew He. Determination of motion parameters and estimation of point correspondences in small nonrigid deformations. *Proc. IEEE Conf. Computer Vision and Pattern Recognition*, pages 943–946, June 1994.

[7] Chandra Kambhamettu, Dmitry B. Goldgof, Demetri Terzopoulos, and Thomas S. Huang. Nonrigid motion analysis. In Tzay Young, editor, *Handbook of PRIP: Computer vision*, volume II, pages 405–430. Academic Press, San Diego, California, 1994.

[8] Jan J. Koenderink and Andrea J. van Doorn. Affine structure from motion. *Journal of Optical Society of America*, 8(2):377–385, February, 1991.

[9] S. A. Kruger and A. D. Calway. A multiresolution frequency domain method for estimating affine motion parameters. *Proceedings of the IEEE International Conference on Image Processing*, pages 113–116, September 1996.

[10] R. Manmatha and John Oliensis. Extracting affine deformations from image patches - i: Finding scale and rotation. *Proceedings of IEEE conference on Computer Vision and Pattern Recognition'93*, pages 754–755, June, 1993.

[11] Robert T. Merrill, W. Paul Menzel, Wayman Baker, James Lynch, and Eugene Legg. A report on the recent demonstration of NOAA's upgraded capability to derive cloud motion satellite winds. *Bull. American Meteorological Society*, 72(3):373–376, March 1991.

[12] Zarina Myles and Niels da Vitoria Lobo. Recovering affine motion and defocus blur simultaneously. *International Conference on Computer Vision and Pattern Recognition (CVPR'96)*, pages 756–763, June 1996.

[13] A. N. Netravali, T. S. Huang, A. S. Krishnakumar, and R. J. Holt. Algebraic methods in 3-d motion estimation from two-view point correspondences. *International Journal of Imaging Systems and Technology*, 1:78–99, 1989.

[14] J. Oliensis. Multiframe structure from motion in perspective. *Workshop on the Representations of Visual Scenes*, pages 77–84, 1995.

[15] K. Palaniappan, Chandra Kambhamettu, A. Frederick Hasler, and Dmitry B. Goldgof. Structure and semi-fluid motion analysis of stereoscopic satellite images for cloud tracking. *Proceedings of the International Conference on Computer Vision*, pages 659–665, 1995.

[16] L. V. Tsap, D. B. Goldgof, and S. Sarkar. Human skin and hand motion analysis from range image sequences using nonlinear fem. *IEEE Nonrigid and Articulated Motion Worshop*, pages 80–89, June, 1997.

[17] Liang Zhao and Chunk Thorpe. Qualitative and quantitative car tracking from a range image sequence. *International Conference on Computer Vision and Pattern Recognition (CVPR'98)*, pages 496–501, June, 1998.